

# Effect of Cu content and temperature on the properties of $\text{Cu}_2\text{ZnSnSe}_4$ solar cells

Sylvester Sahayaraj<sup>1,2,3,a</sup>, Guy Brammertz<sup>2,4</sup>, Marie Buffière<sup>5</sup>, Marc Meuris<sup>2,4</sup>, Jef Vleugels<sup>3</sup>, and Jef Poortmans<sup>1,2,6</sup>

<sup>1</sup> Department of Electrical Engineering (ESAT), KU Leuven, Kasteelpark Arenberg 10, 3001 Heverlee, Belgium

<sup>2</sup> Institute for Material Research (IMO) Hasselt University, Wetenschapspark 1, 3590 Diepenbeek, Belgium

<sup>3</sup> Department of Materials Engineering (MTM), KU Leuven, Kasteelpark Arenberg 44, 3001 Heverlee, Belgium

<sup>4</sup> imec division IMOMECA – partner in Solliance, Wetenschapspark 1, 3590 Diepenbeek, Belgium

<sup>5</sup> Qatar Environment and Energy Research Institute (QEERI), Qatar Foundation, Doha, Qatar

<sup>6</sup> imec – partner in Solliance, Kapeldreef 75, 3001 Leuven, Belgium

Received: 18 April 2016 / Received in final form: 24 June 2016 / Accepted: 29 June 2016

© Sahayaraj et al., published by EDP Sciences, 2016

**Abstract** The complexity involved in obtaining pure Kesterite  $\text{Cu}_2\text{ZnSnSe}_4$  (CZTSe) thin film primarily arises due to its narrow region of stability, leading to the presence of unavoidable binary selenides of the constituent metals. This study offers an insight on the formation of Cu selenides when the amount of Cu is varied in the precursor from Cu poor to Cu rich. The amount of Cu selenides was found to decrease when the composition of CZTSe absorber approached Cu rich conditions but functional devices were not obtained. Detailed characterizations also showed that the Cu and Sn binary phases were present at the backside interface of CZTSe solar cells. However with an increase in the selenization temperature it was found that the amount of Cu selenides and other secondary phases could be drastically minimized or even eliminated leading to high efficiency devices.

## 1 Introduction

Next to Si-based solar cells, inorganic solar cells based on chalcogenide thin films, such as CdTe and  $\text{Cu}(\text{In,Ga})(\text{Se,S})_2$  (CIGS), have been at the forefront in thin film solar cell technology. However, the toxicity of Cd and Te and the reliance on the non-abundant elements In and Ga presents a major barrier towards meeting the multi-terawatt-scale target for renewable energy supplied by photovoltaic cells based on these technologies. Quaternary compounds containing Cu, Zn, Sn and S (CZTS) or Se (CZTSe) are an alternative chalcogenide solar cell absorber that provides diversification away to avoid the non-earth-abundant elements mentioned above. CZT(S,Se) compounds are p-type semiconductors, with high absorption coefficients ( $>10^4 \text{ cm}^{-1}$ ) and direct band gap that varies from 1 eV to 1.5 eV [1, 2] depending on the extent of anion substitution, satisfying the basic requirements for a thin film photovoltaic absorber material. Although recently 12.7% [3] efficiency was achieved with a CZTSSe absorber, the reported values are much lower than record efficiencies obtained with CIGS (22.3%)<sup>1</sup> and

the theoretical Shockley Queisser limits. An important characteristic of high efficiency CZTSe thin film solar cell is a non-stoichiometric composition. The empirical conditions for high-efficiency CZTS(Se) [4, 5] – based thin-film solar cells are the Cu-poor and Zn-rich conditions which would correspond to the A-type or B-type substitution mechanism [6]. Nevertheless, it is worth mentioning that 9.2% devices have also been obtained from Cu rich CZTSe via co evaporation [7]. Among several of the well-known reasons limiting the efficiency of CZTSe based thin film solar cells the existence of a very small region of pure CZTSe in the phase diagram [8], the omnipresent secondary phases such as CuSe,  $\text{Cu}_2\text{Se}$ ,  $\text{SnSe}_2$ ,  $\text{SnSe}$ ,  $\text{ZnSe}$  and  $\text{Cu}_2\text{SnSe}_3$  that evolve during the formation of the quaternary  $\text{Cu}_2\text{ZnSnSe}_4$  due to less tolerance to composition variation [9] have been discussed and well documented [10]. Whether a secondary phase potentially harms the solar cell performance not only depends on the properties of that particular phase but also on its precise location in the active device [11, 12]. Hence, managing these secondary phases during the absorber formation has been a challenging task and has also been a serious limitation in improving the efficiencies of CZTSe solar cells.

In this framework we report on the processing of non-stoichiometric CZTSe thin film solar cells under conditions ranging from Cu poor to Cu rich and the reactive

<sup>a</sup> e-mail: [sahaya@imec.be](mailto:sahaya@imec.be)

<sup>1</sup> [www.pv-magazine.com/news/details/beitrag/solar-frontier-hits-223-on-cigs-cell](http://www.pv-magazine.com/news/details/beitrag/solar-frontier-hits-223-on-cigs-cell).

annealing of the different compositions. Detailed physical and electrical analysis were carried out on the solar cells obtained from these compositions and the results obtained from the physical analysis strongly corroborate with the device characteristics and the processing carried out. Finally a few concerns and limitations are also pointed out.

## 2 Experimental methods

### 2.1 Processing procedure

All the solar cells are fabricated on a 3 mm thick and 25 cm<sup>2</sup> soda lime glass substrate covered by Mo (purchased from Guardian) as electrical back contact. The thickness of Mo is estimated to be 400 nm. The constituent elements that make up the absorber layer are deposited in the order Sn/Zn/Cu on top of Mo by DC sputtering. It is to be noted here that Sn is deposited as Cu<sub>10</sub>Sn<sub>90</sub> alloy in the precursor.

In the final step of the absorber processing, the precursor films are sintered and converted into crystalline CZTSe kesterite layers at high temperatures (450 °C–500 °C). The annealing takes place in a rapid thermal annealing system under a Se rich atmosphere created by a constant flow of 10% H<sub>2</sub>Se in the chamber. The selenization recipe used in this study starts with a fast ramping step at 1 °C/s from room temperature to the maximum selenization temperature followed by a 15 min dwell under H<sub>2</sub>Se flow and finishes with a fast cooling step involving the flow of H<sub>2</sub>/N<sub>2</sub> until the samples are cooled down below 70 °C.

The absorbers are KCN etched (5 wt% solution in aqueous KOH) for 30 or 120 s to remove secondary phases, elemental selenium and native oxide from the absorber surface. The CdS buffer layer is deposited by chemical bath deposition at 70 °C using 2.63 E-3 M Cd(CH<sub>3</sub>CO<sub>2</sub>)<sub>2</sub> and 0.1 M SC(NH<sub>2</sub>)<sub>2</sub> as precursors in aqueous NH<sub>3</sub> medium. The solar cells are finished by a transparent bilayer of RF magnetron sputtered i-ZnO (120 nm) and Al:ZnO (280 nm) followed by the deposition of 1 μm thick Al fingers as front contact. Individual cells with an area of 0.5 cm<sup>2</sup> are laterally isolated by mechanical scribing.

### 2.2 Physical analysis

The morphology and chemical composition of the CZTSe thin films used in this study have been evaluated by SEM-EDX (XL 30 tool, equipped with an EDX analysis system). The accelerating voltage used for the EDX analysis was 20 kV. The Raman spectra were acquired with a Horiba Jobin-Yvon HR800 Raman tool which uses a 532 nm laser with 25% filter. XRD measurements were carried out on a X'Pert Pro MRD X-ray diffractometer in the conventional Bragg-Brentano  $\omega$ -2 $\theta$  geometry using the Cu K $\alpha$  (1.5411 Å) radiation as the incident beam. The cross section SEM Images were obtained from Nova 200 FEI. Depth dependent elemental distribution was investigated by Auger electron spectroscopy. Depth profiles were sputtered in argon gas using a (3 kV × 10 mA) incident beam.

### 2.3 Electrical and optical analysis

The processed solar cells were analyzed using current-voltage (*I-V*, 2401 Sourcemeter, Keithley) measurements performed under a solar simulator system using an AM1.5G spectrum with an illumination density of 1000 W/m<sup>2</sup>. The external quantum efficiency (EQE) has been measured at room temperature using a laboratory-built system with a grating monochromator-based dual-beam setup under chopped light from a Xe lamp. The lifetime of minority carriers was measured using a Hamamatsu C12132 near infrared compact fluorescence lifetime measurement system. The tool uses 15 KHz, 1.2 ns pulsed 532 nm laser and 1 mW of average laser power to illuminate an area of 3 mm diameter on the measured solar cell.

## 3 Results and discussion

### 3.1 Effect of tuning the composition

In this work CZTSe thin films were synthesized by selenization at 450 °C of different Sn/Zn/Cu metallic stacks varying in Cu thickness. From SEM-EDX measurements the [Zn]/[Sn] ratio of these compositions was found to vary between 1–1.1 whilst the [Cu]/([Zn] + [Sn]) ratio in the metallic stack was between 0.44–0.95. The variation in the [Cu]/([Zn] + [Sn]) ratio was achieved by changing the thickness of the Cu layer in the stack. After selenization at 450 °C the [Cu]/([Zn] + [Sn]) ratio of the CZTSe thin films was between 0.53–1.1. The exact reason for the change in the metallic ratios before and after selenization is not fully known. However, Sn or Zn losses cannot be excluded. It is also expected that the initial Cu content might influence the formation of volatile phases resulting in this difference.

Using standard solar cell processing explained in the experimental section CZTSe solar cells were fabricated with these compositions. All 16 compositions could not be studied in detail and in order to differentiate the more relevant samples from the others there are 2 data sets S1 and S2 (Tabs. 1 and 2). The information from S1 is utilized only in Figures 1a and 1b. The differentiation is not based on the Cu content but only to facilitate better understanding of the results.

In all the compositions the presence of binary phases (CuSe, Cu<sub>2-x</sub>Se, SnSe) along with the active CZTSe layer were detected from XRD measurements. All the phases were matched using the PDF cards listed below in the footnote<sup>2</sup>.

Figures 1a and 1b show the plot of the calculated peak area of Cu selenides from several compositions versus the [Zn]/[Sn] and [Cu]/([Zn] + [Sn]) ratios. The  $\Sigma$  CuSe peak area was calculated as the area under the CuSe and Cu<sub>2-x</sub>Se reflections after removing the background

<sup>2</sup> International Center for Diffraction Data: CZTSe – 04-010-6295; MoSe<sub>2</sub> – 04-004-8782; SnSe: 04-009-2274; SnSe<sub>2</sub>: 01-089-2939; ZnSe: 04-015-0312; CuSe: 00-049-1456; Cu<sub>1.8</sub>Se: 04-004-4729; Cu<sub>2</sub>Se: 00-029-0575; Cu<sub>2</sub>SnSe<sub>3</sub>: 04-012-4693; Mo: 01-088-2331.

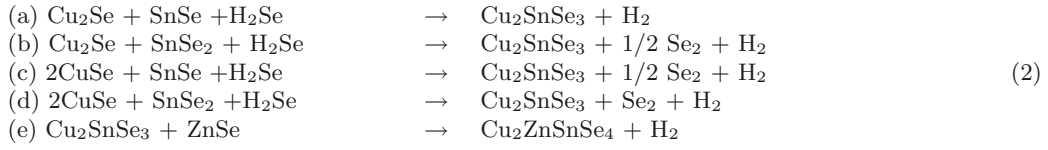
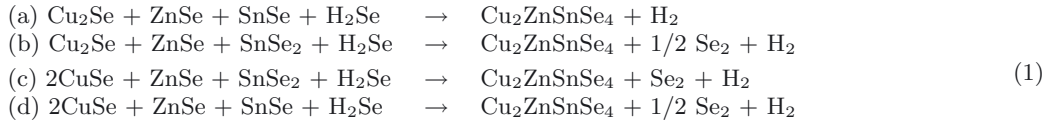
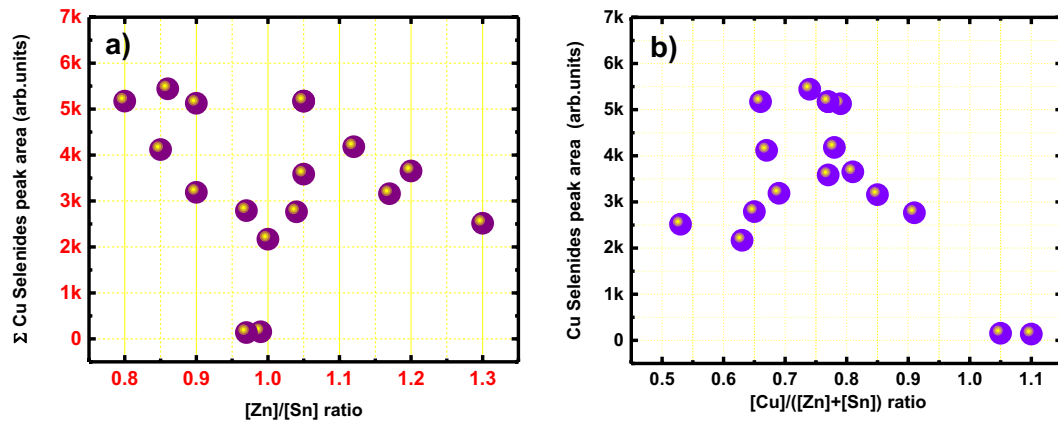


Table 1. Dataset S1.

[Cu]/[Zn]+[Sn]	[Zn]/[Sn]	Efficiency (%)
0.53	1.3	0.9
0.65	1	1
0.66	0.97	2.5
0.67	0.88	3
0.69	0.8	0.8
0.74	0.86	1
0.75	1.05	1.4
0.79	0.91	3.7
0.8	0.91	3.7
0.81	1.2	3.2

Table 2. Dataset S2.

[Cu]/[Zn]+[Sn]	[Zn]/[Sn]	Efficiency (%)
0.76	1.05	6.2
0.77	1.12	6.7
0.84	1.17	6.5
0.91	1.04	6.4
1.05	0.99	0
1.1	0.97	0



**Fig. 1.** Amount of Cu selenides ( $\text{CuSe}$ ,  $\text{Cu}_{2-x}\text{Se}$  and  $\text{Cu}_x\text{Se}$ ) in terms of area under the corresponding XRD peak as a function of (a)  $[\text{Zn}]/[\text{Sn}]$  and (b)  $[\text{Cu}]/([\text{Zn}] + [\text{Sn}])$  ratios measured after selenization at  $450^\circ\text{C}$ .

noise in the XRD measurements and removing the contribution from  $\text{K}\alpha_2$  radiation (note: the peak area was not calculated after a structure refinement and hence, it is not an absolute value and does not relate to the % proportion of the phase in question).

From the available data, a correlation coefficient of  $-0.46$  was calculated between the  $[\text{Cu}]/([\text{Zn}] + [\text{Sn}])$  and the peak area indicating a weak trend whereas no strict correlation was observed between  $[\text{Zn}]/[\text{Sn}]$  ratio and the calculated peak area of Cu selenides.

The reaction leading to the formation of CZTSe has been discussed in literature elsewhere [13]. It can have one of the several pathways (1) and (2) as shown below depending on the composition and the annealing condi-

tions. Both reactions involve the formation of binary selenides of Cu, Sn and Zn (secondary phases) due to their very low formation energies [14–16] even at temperatures below  $300^\circ\text{C}$ .

*See reactions (1) and (2) above.*

The presence of some of the Cu selenide phases after selenization observed in the Cu poor region suggests that the formation reaction of CZTSe is not complete, at least after 15 min of annealing at  $450^\circ\text{C}$ . The CZTSe thin film layers obtained in the Cu poor region were found to contain Cu selenides in different amounts along with the active absorber layer after selenization. For further explanation on the influence of the Cu content on the physical

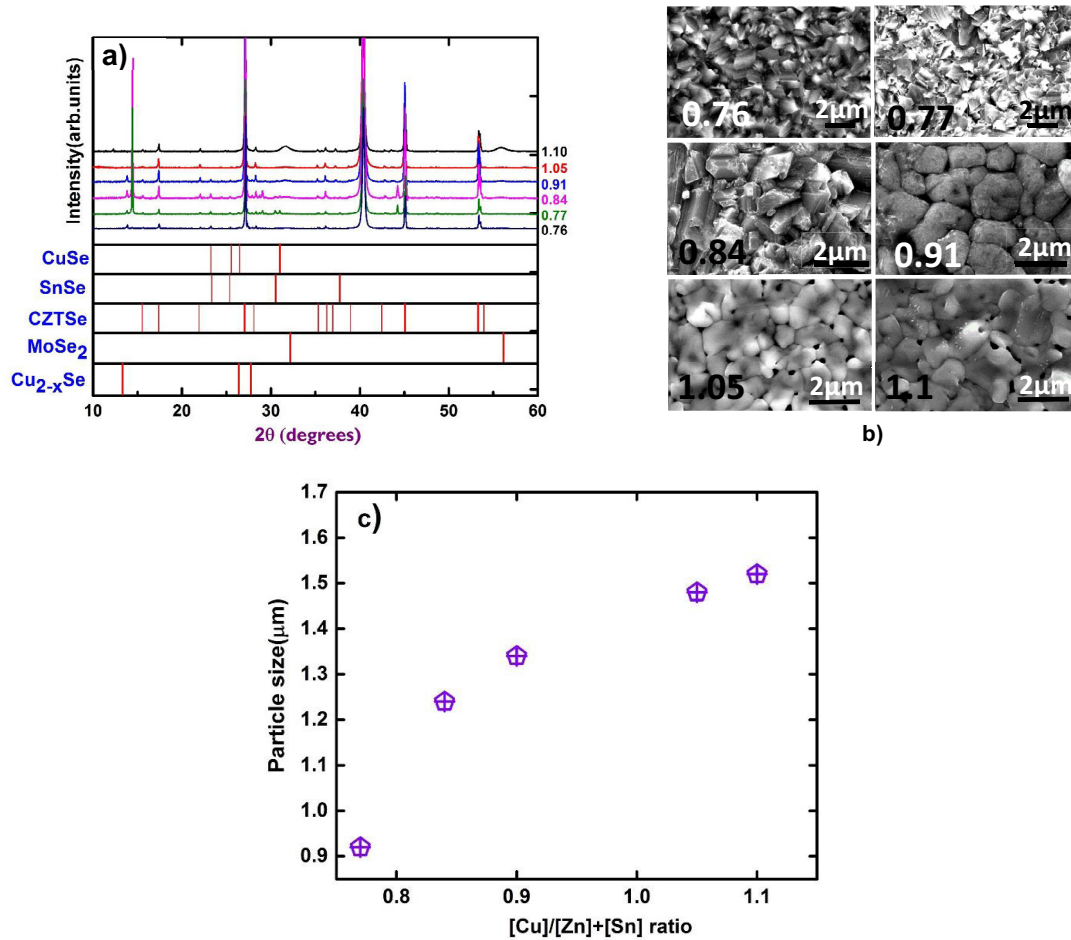


**Fig. 2.** (a) XRD spectrum of CZTSe absorbers with increasing  $[\text{Cu}]/([\text{Zn}] + [\text{Sn}])$  ratios. (b) SEM Images of CZTSe absorbers with increasing  $[\text{Cu}]/([\text{Zn}] + [\text{Sn}])$  ratios. (c) Evolution of particle size with increasing  $[\text{Cu}]/([\text{Zn}] + [\text{Sn}])$  ratio.

and electrical characteristics of CZTSe solar cells, we will further analyse dataset S2 in more detail.

When the Cu content in the starting layers was increased thereby increasing the  $[\text{Cu}]/([\text{Zn}] + [\text{Sn}])$  ratio in the selenized layers the proportion of Cu selenides was found to decrease as mentioned earlier and is also seen from Figure 2a. It is expected to have a lot of Cu selenides in the Cu rich domain but from XRD measurements Cu binaries were not detected (very very small value  $\Sigma$  value in Fig. 1b.) As the  $[\text{Zn}]/[\text{Sn}]$  ratio of the Cu rich absorbers is below 1 it is possible that the existence of  $\text{Cu}_2\text{Se}$  as a stable secondary phase could have been thwarted due to the formation of  $\text{Cu}_2\text{SnSe}_3$  [8]. The increase in the  $[\text{Cu}]/([\text{Zn}] + [\text{Sn}])$  ratio ( $>1$ ) also lead to an increase in the particle size. The word particle size used in this study indicates the respective ferret diameter of the particles measured the from SEM images. This phenomenon in Cu rich conditions has been reported elsewhere [17] for CZT(S,Se) thin films.

Despite the advantage of being morphologically attractive, Cu rich samples never resulted in functional devices. Analysis of these samples by Raman spectroscopy revealed some useful information. Fitting the experimental data with Lorentzian using Origin 2015 Analysis software it

can be seen that for the Cu poor absorbers (Figs. 3a–3c) except the main modes at  $173\text{ cm}^{-1}$  and  $196\text{ cm}^{-1}$  no additional features were observed. Peak fitting of the experimental data for shows Kesterite A modes clearly along with an additional shoulder like feature at  $168.5\text{ cm}^{-1}$  in the Cu rich samples (Figs. 3d and 3e). The peak at  $191.4\text{ cm}^{-1}$  was included to improve the goodness of the fitting procedure. The regression coefficient for the fitting with 3 Lorentzians was almost 1 whereas with 2 Lorentzians it was much lower than 1. Similarly for the Cu rich CZTSe thin films using 4 Lorentzians resulted in a regression coefficient of almost 1 compared to 3 Lorentzians.

In literature the shoulder like feature has been associated with the presence of defects in the crystalline lattice or in some cases these bands arise from non-center phonons, which become active by the relaxation of the quasi crystalline momentum conservation law, caused by the breakage of the crystalline symmetry. In general, either point or extended defects can be responsible for such activation of non-center phonons leading to a characteristic shoulder on the high or low frequency region [18]. This could be an indication of a defective CZTSe phase that forms under Cu rich conditions [19].

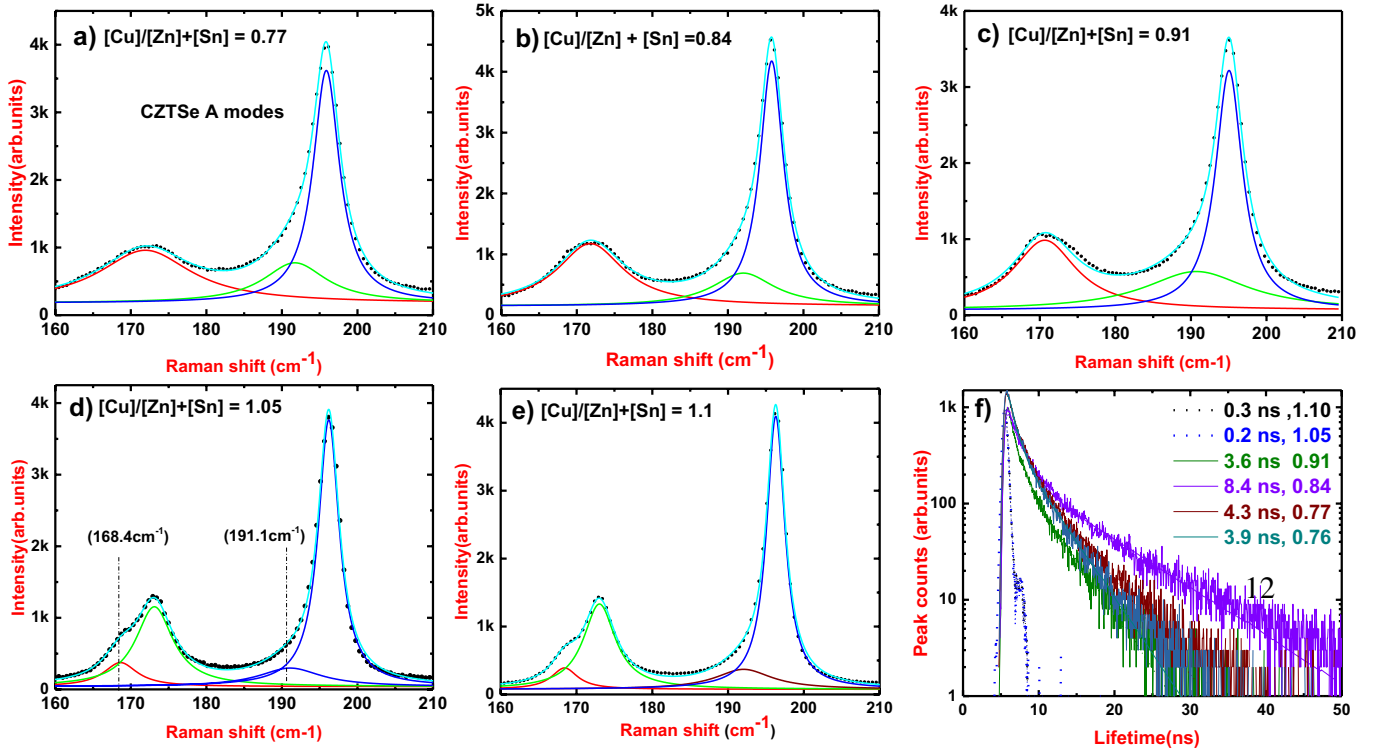


**Fig. 3.** (a)–(c) Detailed peak fitting of Kesterite A modes of Cu poor CZTSe thin film absorber (d) and (e) Detailed peak fitting of Kesterite A modes of Cu rich CZTSe thin film absorber. (f) Comparison of the minority carrier lifetimes of Cu poor and Cu rich samples in this study.

The minority carrier lifetime extracted from time resolved photoluminescence measurement performed on these samples is shown in Figure 3f. The minority carrier lifetimes were measured at room temperature. The minority carrier lifetime is derived using a two exponential fit to the photoluminescence decay curve. The slower decay time usually is considered as the minority carrier lifetime [20]. It can be seen that the carrier lifetimes are very low for the Cu rich samples in comparison with the lifetime of the other Cu poor samples. The exact reason for the very low lifetimes remains unknown, but probably involves electronic defect states.

In order to understand the effect of the Cu selenides on CZTSe devices, we selected 2 Cu poor compositions (as no working devices could be obtained from Cu rich) which have a  $[\text{Cu}]/([\text{Zn}] + [\text{Sn}])$  ratio of 0.76 and 0.77 in the thin film after selenization. The same  $5 \times 5 \text{ cm}^2$  metallic stack that was selenized at  $450^\circ \text{C}$  for both compositions was cut in 2 pieces and one of them was processed into a full solar cell without the KCN etching step while the other half was processed with the KCN etching step. The illuminated IV curves are shown in Figures 4a and 4b for comparison. The solar cell processed without the KCN step suffered from low shunt resistances (4 times lower) and a lower  $V_{oc}$  than the solar cell that had the KCN etching step. Also Figures 4e and 4f show the presence of CuSe after KCN etching in these devices. The variation in FF in the 2 solar cells is due to the change in the Shunt resistance. Similar to the change in shunt resistance, the secondary

phases shown (CuSe and SnSe) could also act as potential recombination centers thereby decreasing the  $V_{oc}$ .

It seems logical to increase the KCN etching time to achieve complete removal of these phases but longer KCN etching times are associated with a progressive decrease of the FF of the solar cells when increasing the treatment duration from 30 s to 300 s as reported by Buffiere et al. [21]. Hence, keeping this in mind longer etching times were avoided.

The AES depth profile of a 6.7% solar cell (KCN etched) shown in Figure 4c shows a clear increase in the Cu and Se signals compared to the Sn and Zn signals which keep going down at the same time. A small but an observable increase in the Cu and Se signals in the absorber at the backside at the same time can indicate the presence of an inclusion like CuSe along with CZTSe. As the amount of this phase is not so high only a small difference could be observed.

Similarly the depth profile of the 6.2% device (KCN etched) seen in Figure 4d shows an increase in the Sn and Se signals compared to the Cu and Zn signals which keep going down at the same time. A small but an observable increase in the Sn and Se signals in the absorber at the backside at the same time can indicate the presence of an inclusion like SnSe along with CZTSe.

From the depth profiles of these 2 high performance devices obtained in this study shown here it is fair enough to say that secondary phases that are responsible for this shunting behavior (CuSe or SnSe) are present most likely

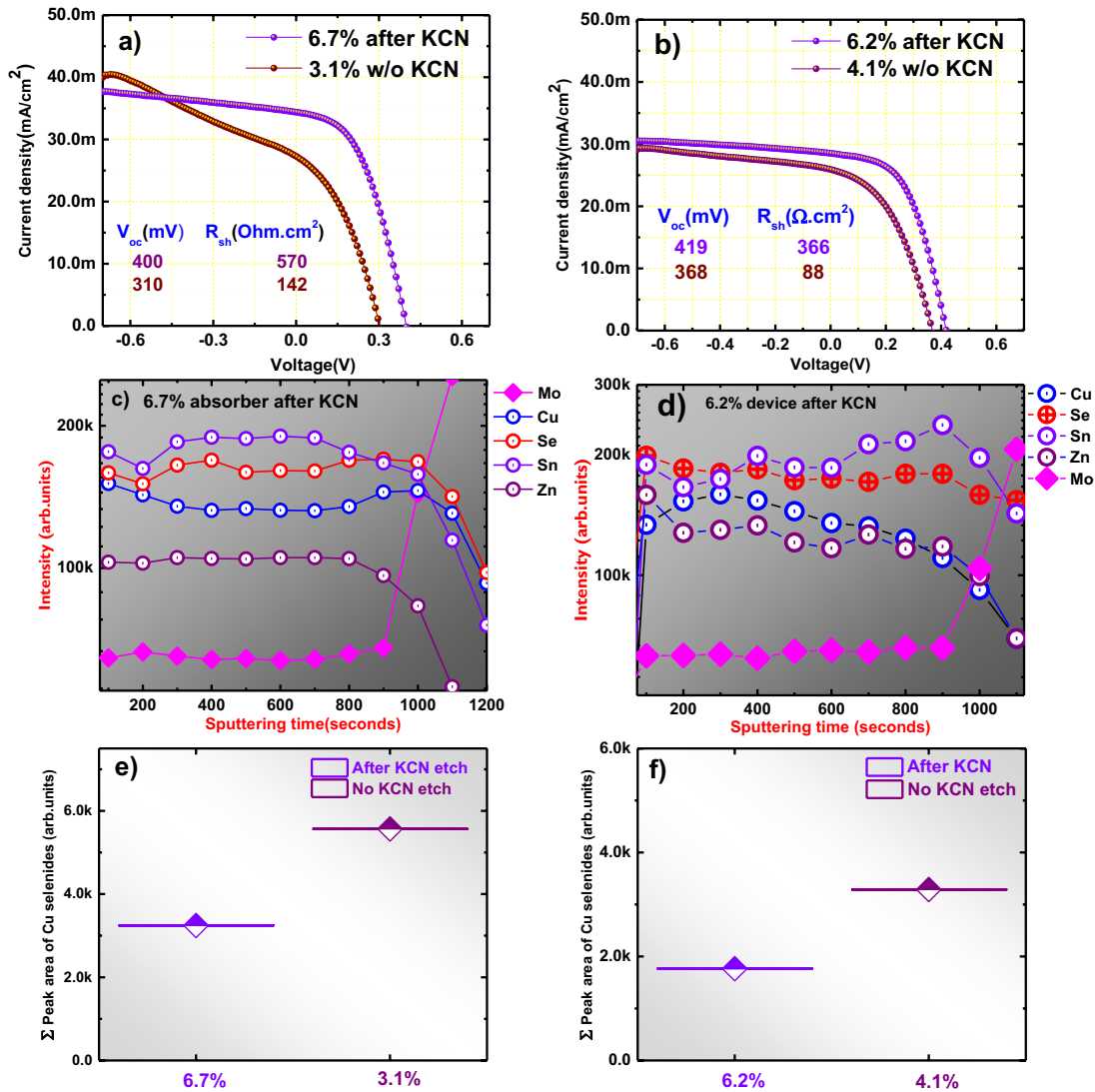


**Fig. 4.** (a) and (b) Illuminated  $I-V$  curves of CZTSe solar cells fabricated with and without KCN etching step. (c) and (d) AES depth profiling of the same cells. (e) and (f) graphical schematic showing the amount of Cu selenide secondary phase in the 2 solar cells.

towards the backside of the completed device. Given that the absorber is Cu poor, if these secondary phases had segregated near the surface it would have been etched by KCN quite considerably. Since this did not take place CuSe might exist as a buried phase in the active absorber in Cu poor conditions. As KCN etching will not help in overcoming this problem another alternative has to be sought after.

### 3.2 Effect of temperature

During the processing of the absorber the selenization temperature was found to have the same effect as Cu rich films on the grain growth. When the selenization temperature was increased from 450 °C to 500 °C the measured grain size of CZTSe (measured as the ferret diameter) also showed an increase. Figure 5 clearly illustrates this observation on the data set S2.

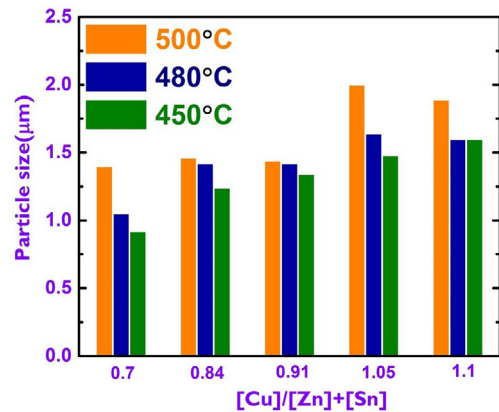


**Fig. 5.** Schematic showing the evolution of particle size with temperature for different  $[\text{Cu}]/([\text{Zn}] + [\text{Sn}])$  ratios. (The ferret diameter could not be measured for the CZTSe absorber with  $[\text{Cu}]/([\text{Zn}] + [\text{Sn}])$  ratio 0.77 and hence, it is not shown here).

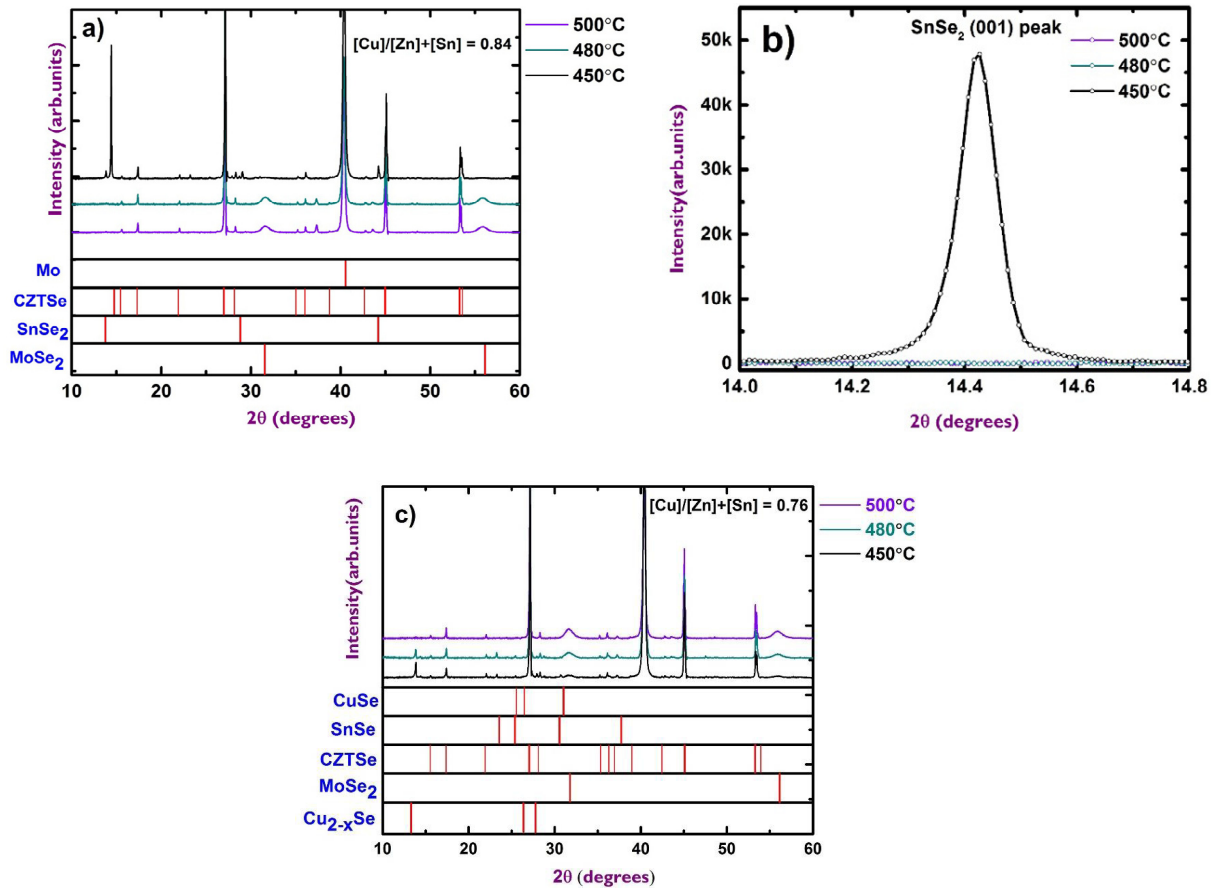


**Fig. 6.** (a) XRD spectrum of CZTSe thin film absorber with  $[\text{Cu}]/[\text{Zn}] + [\text{Sn}]$  ratio of 0.84 selenized at 450 °C, 480 °C and 500 °C. (b) Section showing the disappearance of the intense (001) peak of  $\text{SnSe}_2$ . (c) XRD spectrum of CZTSe thin film absorber with  $[\text{Cu}]/[\text{Zn}] + [\text{Sn}]$  ratio of 0.76 selenized at 450 °C, 480 °C and 500 °C.

As Cu rich films did not result in good devices, and all other Cu poor CZTSe absorbers selenized at temperatures 480 °C and 500 °C peeled off after KCN etching except the ones with 0.84 and 0.76 further discussion within this section is limited to these two absorbers. Figures 6a and 6c show the XRD measurements of these CZTSe absorbers. Figure 6a shows the XRD spectrum of the CZTSe thin film layer with  $[\text{Cu}]/([\text{Zn}] + [\text{Sn}])$  ratio of 0.84 along with  $\text{SnSe}_2$  secondary phase indexed within the measurement range at 450 °C. As the selenization temperature was increased from 450 °C, the disappearance of  $\text{SnSe}_2$  binary phase can be observed. The intense (001) peak, the (011) and the (003) peaks of  $\text{SnSe}_2$  completely disappears at 480 °C itself as evidenced from the Figure 6b.

Figure 6c shows the XRD spectrum of the CZTSe thin film layer with  $[\text{Cu}]/([\text{Zn}] + [\text{Sn}])$  ratio of 0.76. At 450 °C the presence of  $\text{CuSe}$ ,  $\text{SnSe}$  and  $\text{Cu}_x\text{Se}$  (probably in small amounts) along with CZTSe can be observed. With the increase in the selenization temperature the secondary phases were found to react reaching completion identical to the CZTSe absorber discussed formerly. Applying the phase diagram of CZTSe discussed in [8] to the pure selenide we can find out that except  $\text{ZnSe}$ , all other phases seen from the XRD measurements of these thin

film layers phases such as  $\text{Cu}_{2-x}\text{Se}$  (stable in the Cu rich region) and  $\text{SnSe}_2$  (stable in the Sn rich region) are not the stable secondary phases in the Cu poor and Zn rich regions. Hence, an increase in the selenization temperature helps in improving the kinetics of the overall reaction enabling complete reaction of all the binary selenides that are present at 450 °C and below.

This effect of selenization temperature is also reflected in the solar cell performance. Figures 7a and 7c show the illuminated IV curves of the solar cells made from the absorbers with  $[\text{Cu}]/[\text{Zn}] + [\text{Sn}]$  ratios of 0.84 and 0.76. The solar cells which were processed with CZTSe selenized at a higher temperature showed a better overall performance. From Figures 7b and 7d we see that the carrier collection efficiency has significantly improved for solar cells processed with CZTSe selenized at 480 °C pointing out clearly that higher selenization temperatures are needed for obtaining higher efficiencies in CZTSe based solar cells but the problem of delamination of the active absorber material processed at higher temperatures during the KCN etching step is a real limitation in achieving this. The delamination after KCN etching could arise due to the poor adhesion of the absorbers at the Mo backside interface at higher temperatures but addressing such issues is beyond the scope of this work.

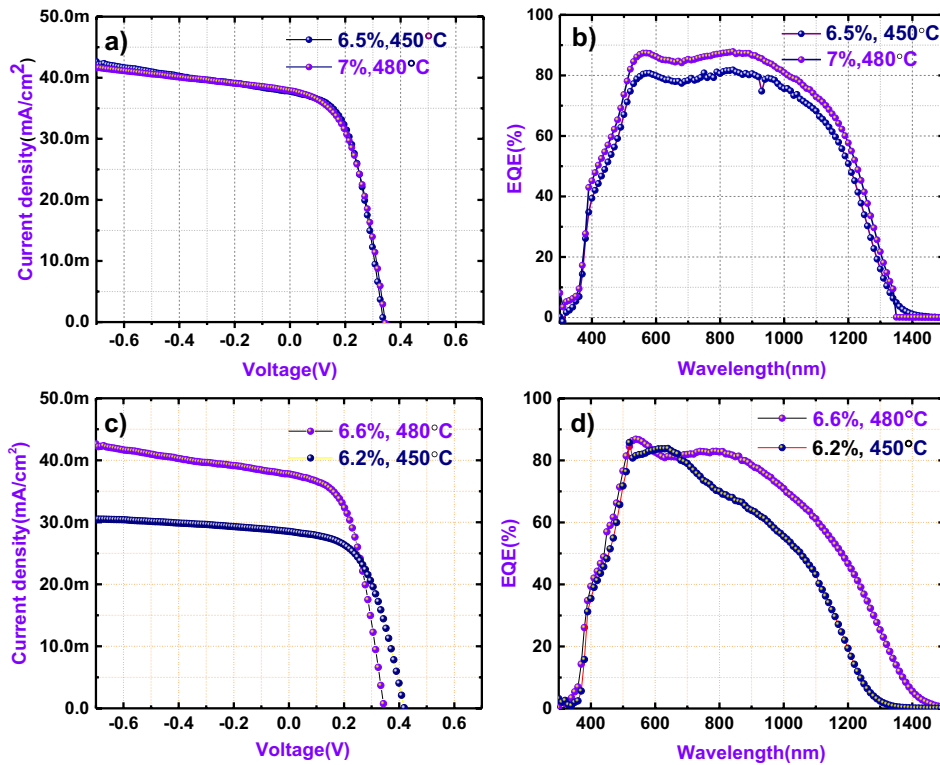


**Fig. 7.** (a) and (c) Illuminated IV curves of CZTSe solar cells with a  $[\text{Cu}]/[\text{Zn}] + [\text{Sn}]$  ratio of 0.84 and 0.76 selenized at 450 °C and 480 °C respectively (b) and (d). External Quantum efficiency curves of CZTSe solar cells with a  $[\text{Cu}]/[\text{Zn}] + [\text{Sn}]$  ratio of 0.84 and 0.76 selenized at 450 °C and 480 °C respectively.

## 4 Conclusions

The effects of varying the Cu content during the processing of CZTSe absorbers and varying the selenization temperature were investigated. While Cu rich samples turn out to be an interesting option due to their attractive grain morphology, very low lifetimes and electronic defect states lead to nonfunctional devices. As already shown in all previous literature data, we reconfirm the finding that the best composition range for making good devices seems to be Cu poor between 0.75 and 0.85 for a Zn rich interval 1.1–1.2. In this composition range we have been able to make solar cell devices with an efficiency of up to 7%. But even in this composition interval numerous secondary phases could be observed, which shows that the formation reaction for CZTSe is not complete. Nevertheless it was also found that, the amount of secondary phases in this region can be strongly decreased by increasing the selenization temperature most likely at the expense of exacerbating the adhesion between the Mo/CZTSe interface. Hence, obtaining CZTSe absorbers at higher temperatures in the right composition window and ensuring good adhesion between the absorber and the backside metal is a meaningful direction to proceed in, to obtain a good quality CZTSe absorber and eventually solar cells.

This research is partially funded by the Flemish government, Department Economy, Science and Innovation. We would like

to acknowledge Flamac at Gent for the sputter-deposition of the metal layers.

## References

1. S. Siebentritt, S. Schorr, *Prog. Photovolt.: Res. Appl.* **20**, 512 (2012)
2. C. Persson, *J. Appl. Phys.* **107**, 053710 (2010)
3. J. Kim, H. Hiroi, T. Todorov, T.O. Gunawan, M. Kuwahara, T. Gokmen, D. Nair, M. Hopstaken, B. Shin, Y.S. Lee, W. Wang, H. Sugimoto, D.B. Mitzi, *Adv. Mater.* **26**, 7427 (2014)
4. I. Repins, C. Beall, N. Vora, C. DeHart, D. Kuciauskas, P. Dippo, B. To, J. Mann, W.C. Hsu, A. Goodrich, R. Noufi, *Sol. Energy Mater. Sol. Cells* **101**, 154 (2012)
5. Yun Seog Lee, T. Gershon, O. Gunawan, T.K. Todorov, T. Gokmen, Y. Virgus, *Supratik Adv. Energy Mater.* **5**, 1401372 (2014)
6. L. Choubac, A. Lafond, C. Guillot-Deudon, Y. Moelo, S. Jobic, *Inorg. Chem.* **51**, 3342 (2011)
7. W.C. Hsu, I. Repins, C. Beall, C. DeHart, T. Bobby, W. Yang, Y. Yang, R. Noufi, *Prog. Photovolt.: Res. Appl.* **22**, 35 (2014)
8. I.D. Olekseyuk, I.V. Dudchak, L.V. Piskach, *J. Alloys Compd.* **368**, 135 (2004)
9. T. Tanaka, T. Sueishi, K. Saito, Q. Guo, M. Nishio, K. Yu, V. Walukiewicz, *J. Appl. Phys.* **111**, 053522 (2012)

10. J. Just, D. Lutzenkirchen-Hecht, R. Frahm, S. Schorr, T. Unold, *Appl. Phys. Lett.* **99**, 262105 (2011)
11. A. Redinger, K. Hönes, X. Fontaneì, V. Izquierdo-Roca, E. Saucedo, E. Valle, A. Peìrez-Rodrìguez, S. Siebentritt, *Appl. Phys. Lett.* **98**, 101907 (2011)
12. G. Brammertz, S. Oueslati, M. Buffière, J. Bekaert, H. El Anzeery, K.B. Messaoud, S. Sahayaraj, T.Nuytten, C. Koble, M. Meuris, J. Poortmans, *IEEE J. Photovolt.* **5**, 649 (2015)
13. M. Ganchev et al., *Thin Solid Films* **519**, 7394 (2011)
14. D. Cahen, *J. Phys. Chem. Solids* **53**, 991 (1992)
15. S. Boone, O.J. Kleppa, *Thermochimica Acta* **109**, 197 (1992)
16. T.B. Massalski, *Binary Alloy Phase Diagrams*, 2nd edn. (ASM International, 1990)
17. G. Suresh Babu et al., *Sol. Energy Mater. Sol. Cells* **94**, 221 (2010)
18. *Advanced Characterization Techniques for Thin Film Solar Cells*, edited by D. Abou-Ras, T. Kirchartz, U. Rau (Wiley VCH, 2011)
19. M. Dimitrievska, A. Fairbrother, A. Perez-Rodriguez, E. Saucedo, V. Izquierdo-Roca, *Acta Mater.* **70**, 272 (2014)
20. A. Kanevce, D.H. Levi, D. Kuciauskas, *Prog. Photovolt.: Res. Appl.* **22**, 1138 (2014)
21. M. Buffière et al., *ACS Appl. Mater. Interfaces* **7**, 14690 (2015)

**Cite this article as:** Sylvester Sahayaraj, Guy Brammertz, Marie Buffière, Marc Meuris, Jef Vleugels, Jef Poortmans, Effect of Cu content and temperature on the properties of Cu<sub>2</sub>ZnSnSe<sub>4</sub> solar cells, *EPJ Photovoltaics* **7**, 70304 (2016).